17[th] World Conference on Earthquake Engineering, 17WCEE

Sendai, Japan - September 13th to 18th 2020

TOPOLOGY OPTIMIZATION OF REPLACEABLE COMPONENTS TO REDUCE DEFORMATION IN STRUCTURAL WALLS

Wenjun Gao[(1)], Xilin Lu [(2)]

[(1)] *PhD student; State Key Laboratory of Disaster Reduction in Civil Engineering, Tongji University, Shanghai 200092, China; e-mail address: 2014Joker@tongji.edu.cn*

[(2)] *Professor; State Key Laboratory of Disaster Reduction in Civil Engineering, Tongji University, Shanghai 200092, China; e-mail address: lxlst@tongji.edu.cn*

Abstract

Replaceable-component structures behave as conventional structures to resist lateral loads under minor earthquakes and require that the damage caused by strong earthquakes is only restricted in replaceable zones, whereas primary structural members remain intact. Consequently, damaged buildings can be resumed and normally operate within a very short time by only replacing damaged components which also play the role of passive energy-dissipation devices to dissipate input energy. The concept of replacement has been widely applied in beam-column joints of frames, as well as coupling beams of coupled structural walls. Apart from coupling beams which are the most vulnerable structural components, the bottom of a structural wall also easily incurs severe damage such as spalling or crushing of concrete, also buckling, yielding and fracture of longitudinal rebars. A straightforward problem-solving approach is to substitute replaceable components for brittle reinforced concrete parts at the bottom corners. Despite the achieved improvements, the design of replaceable components still relies on engineering intuition and a trial and error strategy to expect that replaceable components suffer from damage prior to the reinforced concrete region so that the remaining reinforced concrete parts are protected as far as possible. However, existing experimental results demonstrated that purely enlarging the section dimensions of structural members or simply adding auxiliary components still possibly leads to undesired local brittle failure. An inherent trade-off between the stiffness from replaceable components and that from reinforced concrete region is observed. Too strong replaceable components probably remain elastic and cause damage transfer to the reinforced concrete region, which violates the design goal of replaceable components. Conversely, too weak replaceable components have trivial contribution to the lateral resistance, thereby the lateral loads resisted by the reinforced concrete region is many times larger than that resisted by replaceable components. As a result, the reinforced concrete parts are prone to be damaged instead of replaceable components.

In this study, the tough design problem is formulated into a minimization problem from the perspective of topology optimization that has been thriving from 1988 and extensively applied in manufacturing and architecture industries to enhance structural performance. The design goal is to suppress the maximum deformation in the reinforce concrete region, since severe deformation is a prerequisite for brittle failure of concrete. Addressing deformation in the form of strain tensor may lead to complicated systems and formulations. Instead, element strain energy as a scalar is used to quantify deformation intensity in each element. To avoid numerical instability, the aggregation method is utilized to approximate the maximum element strain energy. The objective function in the form of the aggregated value is minimized in the proposed optimization scheme which is driven by sensitivities of design variables in a gradient-based algorithm. In optimization process, an initial design consisting of intermediate elements gradually involves into the optimum design using solid elements to form the profile of replaceable components. Optimization results are presented to demonstrate the effectiveness of the proposed optimization scheme. Also, several factors that affect optimization results are investigated.

Keywords: replaceable components; structural walls; earthquake resilience; topology optimization; finite element method

1. Introduction

The collapse of building structures has been effectively controlled by conventional ductility design that had been attracting attention in the 1990s and 2000s to reduce the casualties in severe earthquakes. Since ductility design allows plasticity to develop in structural components, buildings inevitably suffer from residual deformation and damage with varying degrees when strong earthquakes hit cities. Yet, there hitherto are no well-defined guidelines for the assessment and estimation of residual deformation and plastic damage. It is very difficult to repair or estimate the capacity and safety of damaged building structures. To ensure safety, follow-up demolishment and reconstruction still cause huge economic loss. Resilient design [1] which targets this problem by emphasizing the restorability of structures is becoming a main-stream design philosophy. This concept derives two promising structural systems: self-centering structures and replaceable-component structures. Self-centering walls [2, 3], frames [4, 5] and piers [6] are capable of returning to their original positions with minor damage and negligible residual deformation. In this way, self-centering structures not only ensure safety, but also avoid temporary suspension of lifetime engineering [7]. Although advanced numerical models have been proposed by researchers [8, 9] to capture the self-centering behavior, it still needs a sophisticated design procedure [10] to stand the extraordinary seismic performance out. Unlike self-centering structures towards being free of damage, replaceable-component structures behave as conventional structures to resist lateral forces under minor earthquakes but require that the damage caused by strong earthquakes is only restricted in replaceable zones, whereas primary structural parts remain intact. Consequently, damaged buildings can be resumed and normally operate within a very short time by replacing damaged components which also play the role of passive energy-dissipation devices to dissipate input energy.

The concept of replacement has been widely applied in beam-column joints of frames [11], as well as coupling beams of coupled structural walls [12, 13, 14]. Apart from coupling beams which are the most vulnerable structural components, the bottom of a structural wall also easily incurs sever damage such as spalling or crushing of concrete, also buckling, yielding and fracture of longitudinal rebars [15]. Indeed, other failure modes of reinforced concrete structural walls were observed from post-earthquake events' reconnaissance [16, 17] or controlled experiments [18, 19]. However, the structural walls with a high aspect ratio in tall buildings are dominated by flexural behavior, provided the structural designs strictly follow existing criteria that require higher shear capacity in comparison with flexural capacity to avoid brittle failure. The flexural failure of structural walls observed in experiments [15, 16, 20] starts from horizontal cracks appearing at the bottom of the boundary parts, which is followed by the initial yielding of the longitudinal reinforcement near the pedestal. This phenomenon is also verified by numerical simulation results [21] in which the stresses in the compression boundary elements are about ten times greater than those in the panel.

It is extremely hard to repair these damaged bottom corners in conventional structural walls, due to the material properties of concrete and steel bars. A straightforward problem-solving approach first proposed by Lu et al. [22] is to substitute replaceable components for original reinforced concrete parts at the bottom corners. It has been found that the replaceable components should be designed more reasonably, otherwise the stiffness of the tested structural wall decreased very fast after its drift exceeded 0.3%. Better seismic performance of structural walls in the literature [23] utilized steel struts to play the role of replaceable components at the bottom corners. Despite the achieved improvements, the design of replaceable components still relies on engineering intuition and a trial and error strategy.

This paper attempts to investigate reasonable designs of replaceable components in structural walls from the perspective of topology optimization that has been thriving from 1988 [24] and extensively applied in manufacturing [25] and architecture industries [26] to enhance structural performance. The configuration of replaceable components is optimized to suppress the maximum deformation in the reinforced concrete region. The optimization process is driven by the sensitivities of design variables. In the topology optimization process, an initial design consisting of intermediate elements gradually involves into the optimum design where solid elements constitute the profile of replaceable components.

2. Strength balance in adding auxiliary components

Attempts have been made to yield a desired failure mode in structural joints by adding auxiliary haunches [27, 28, 29]. As shown in Fig. 1, the internal forces in beam-to-column assemblies are significantly altered by installing metallic haunches. The maximum moment is relocated away from the original critical sections to the position where haunches are connected to beams. Owing to this adjustment re-coordinating the stiffness relation between structural components, damage occurs at beams, but columns remain intact. Hence, brittle failure or yielding at beam-to-column joints or column members is avoided.

However, damage and failure still relocate to other structural members. Difficulties in repairing these damaged structural members are prohibitive. Similar auxiliary haunches cannot be directly installed at the bottom of a reinforced concrete structural wall to play the role of replaceable components. It is because that resulting damage still possibly develops in the reinforced concrete region, whereas auxiliary haunches may remain elastic. It violates the design philosophy of replaceable components. Theoretically, replaceable components are expected to be damaged prior to structural members.

Two aspects lead to this violation: the installed auxiliary haunches are too strong compared with other structural members on the one hand, the installed haunches cause stress concentration elsewhere on the other hand. For the first aspect, the opposite side, i.e. too weak auxiliary components, still could be problematic, since the fuse effect provided by auxiliary components becomes trivial. Hence, there is a complex trade-off when designing auxiliary components to satisfy the replaceable requirements.

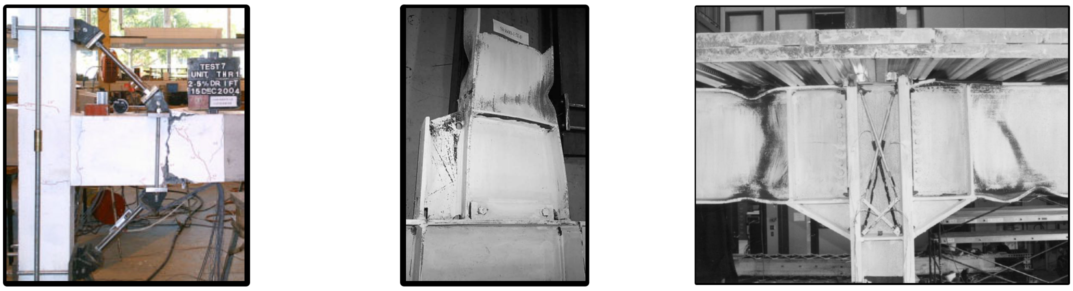

(a) (b) (c)

Fig. 1 – Auxiliary haunches in beam-to-column joints and resulting failure modes: (a) [27]; (b) [28]; (c) [29].

3. Topology optimization

3.1 Numerical models

This section introduces the modelling scheme, which brings simplicity but captures essential physics. Fig. 2(a) visualized a conventional structural wall specimen in the literature [23]. The geometric dimensions of the numerical wall model are denoted as H_{W} in height, B_{W} in width and t_{c} in thickness. In following investigation, the variation of H_{W} leads to different aspect ratios, whereas B_{W} and t_{c} are fixed as 1200mm and 140mm, respectively. The vertical loads $\boldsymbol{F}_{\mathrm{N}}$ and lateral loads $\boldsymbol{F}_{\mathrm{V}}$ are uniformly applied along the top edge. The sum of lateral loads is 150kN, while the sum of vertical loads is determined according to the ratio of axial compression stress to strength δ_{N} which is defined by $\delta_{\mathrm{N}} = \sum \boldsymbol{F}_{\mathrm{N}} / (f_{\mathrm{c}} t_{\mathrm{c}} B_{\mathrm{W}})$. Herein, f_{c} = 26.8MPa is the design value of concrete compressive strength. The bottom edge is fully fixed. Considering symmetry and anti-symmetry, the original structure in Fig. 2(a) can be simplified as the half structure in Fig. 2(b) and (c) with symmetric loads and anti-symmetric loads. This simplification reduces computational cost in following finite element analysis and optimization. Note that boundary conditions should be consistent with applied loads in the half structure. The numerical model used for optimization consists of passive domain Ω_{P} and active domain Ω_{A} as illustrated in Fig. 2(b). The passive domain represents the half structure of a structural wall, whereas the active domain is the background to yield potential configurations of replaceable components. The geometric dimensions of the active domain are denoted as H_{W} in height, B_{A} = 1200mm in width and t_{s} = 8mm in thickness.

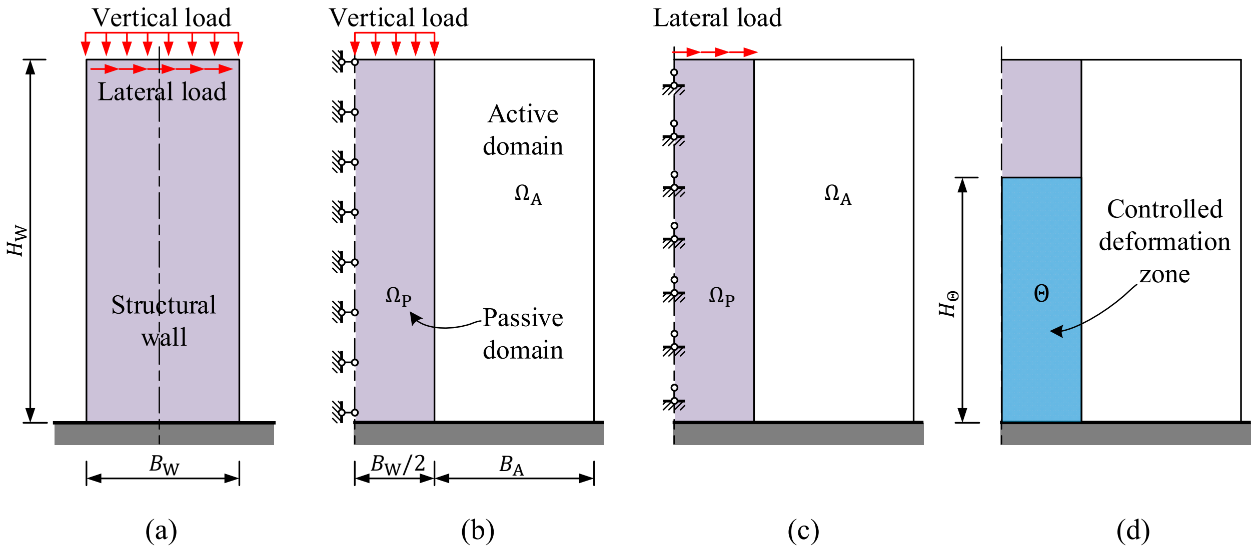

Fig. 2 – Schematics of numerical modes.

The Young's modulus and Poisson's ratio for the passive domain are E_c = 33GPa and μ_c = 0.23, and those for the active domain are E_s = 200GPa and μ_s = 0.30. Only deformation in the controlled deformation zone Θ is concerned and controlled in optimization process, since the bottom region suffers from severer deformation. The entire design domain is uniformly discretized by square bilinear in-plane stress elements with an element length of 15mm. Structural response under applied loads is solved under small deformation assumption. The corresponding static equilibrium follows

$$\begin{aligned}
&\boldsymbol{K}\boldsymbol{U}_{\mathrm{N}} = \boldsymbol{F}_{\mathrm{N}}, \qquad \boldsymbol{K}\boldsymbol{U}_{\mathrm{V}} = \boldsymbol{F}_{\mathrm{V}} \\
&\boldsymbol{U} = \boldsymbol{U}_{\mathrm{V}} + \boldsymbol{U}_{\mathrm{N}}, \qquad \boldsymbol{K} = \boldsymbol{K}_{\mathrm{c}} + \boldsymbol{K}_{\mathrm{s}} \\
&\boldsymbol{K}_{\mathrm{c}} = \sum_{e\in\Omega_{\mathrm{P}}} \boldsymbol{K}_{\mathrm{c},e}, \qquad \boldsymbol{K}_{\mathrm{s}} = \sum_{e\in\Omega_{\mathrm{A}}} \boldsymbol{K}_{\mathrm{s},e} \\
&\boldsymbol{K}_{\mathrm{s},e} = t_{\mathrm{s}} \int_{A_e} \boldsymbol{B}_{\mathrm{L0}}^{\mathrm{T}} \boldsymbol{D}_{\mathrm{s},e} \boldsymbol{B}_{\mathrm{L0}}\, \mathrm{d}A = E_{\mathrm{s},e} t_{\mathrm{s}} \overline{\boldsymbol{K}}_e \\
&\boldsymbol{K}_{\mathrm{c},e} = t_{\mathrm{c}} \int_{A_e} \boldsymbol{B}_{\mathrm{L0}}^{\mathrm{T}} \boldsymbol{D}_{\mathrm{c},e} \boldsymbol{B}_{\mathrm{L0}}\, \mathrm{d}A = E_{\mathrm{c}} t_{\mathrm{c}} \overline{\boldsymbol{K}}_e \\
&\overline{\boldsymbol{K}}_e = \int_{A_e} \boldsymbol{B}_{\mathrm{L0}}^{\mathrm{T}} \overline{\boldsymbol{D}} \boldsymbol{B}_{\mathrm{L0}}\, \mathrm{d}A
\end{aligned} \tag{1}$$

where $\boldsymbol{K}_{\mathrm{c}}$ and $\boldsymbol{K}_{\mathrm{s}}$ represent the stiffness matrices originating from the passive domain and the active domain, respectively; $\boldsymbol{U}$ is the displacement vector corresponding to $\boldsymbol{F}_{\mathrm{N}} + \boldsymbol{F}_{\mathrm{V}}$; $\overline{\boldsymbol{D}}$ is the normalized element constitutive matrix; $\boldsymbol{B}_{\mathrm{L0}}$ is the linear strain-displacement transformation matrix c.f. Table 6.5 in [30]; $E_{\mathrm{s},e}$ is the Young's modulus of elements in the active domain and should be determined according to the following interpolation scheme; A_e is the in-plane area of element e.

3.2 Interpretation scheme

A "density-based topology optimization approach", which followed [24, 31] and became an efficient form [32, 33], is employed to turn a 0-1 distribution problem into a continuous distribution problem. A design variable $\rho_e \in [0,1]$ is assigned to each element. The material Young's modulus $E_{\mathrm{s},e}$ for each element can be directly related to the projected physical density $\bar{\rho}_e$ according to the modified Solid Isotropic Material with Penalization (SIMP) approach [34] as

$$E_{\mathrm{s},e} = E_{\mathrm{s,min}} + \bar{\rho}_e^{q}\left(E_{\mathrm{s}} - E_{\mathrm{s,min}}\right) \tag{2}$$

where $q \geq 0$ is the penalty parameter ($q = 3$ in this study); $E_{\mathrm{s,min}} = 10^{-9}E_{\mathrm{s}}$ is a very small value and assigned to void elements ($\bar{\rho}_e = 0$) in order to prevent global stiffness matrix from becoming singular; $\bar{\rho}_e$ is the projected physical density [35] calculated by

$$\bar{\rho}_e = \frac{\tanh(\beta_{\mathrm{f}}\eta) + \tanh\big(\beta_{\mathrm{f}}(\tilde{\rho}_i - \eta)\big)}{\tanh(\beta_{\mathrm{f}}\eta) + \tanh\big(\beta_{\mathrm{f}}(1 - \eta)\big)} \tag{3}$$

where η and β_{f} control the shape of Eq. (3) by gradually increasing β_{f} during the optimization process; $\tilde{\rho}_e$ is the filtered density of element e, which is calculated as

$$\tilde{\rho}_e = \frac{1}{\sum_{i \in n_e} H_{e,i}} \sum_{i \in n_e} (\rho_e H_{e,i}) \tag{4}$$

where n_e is the set of element i for which the center-to-center distance $\Delta(e,i)$ to element e is smaller than the filter radius r_{min}, and $H_{e,i}$ is a weight factor defined as $H_{e,i} = \max\big(0, r_{\mathrm{min}} - \Delta(e,i)\big)$. Herein, r_{min} spans a length of 5 elements. Due to the modified SIMP scheme, $\boldsymbol{K}_{\mathrm{s},e}$ in Eq. (1) is readily connected to design variables. In contrast, the interpolation of element volume is based on a linear form, i.e. $V_e = \bar{\rho}_e V_{0,e}$, where $V_{0,e}$ is the volume of element e in a solid state.

3.3 Formulation

Strain energy is used as a straightforward quantity to measure element deformation. Similar strategy can also be found in previous researches [36, 37]. As a scaler, strain energy is independent of directions, and therefore complexity caused by handling strain tensor is avoided. The original objective is to minimize the maximum element strain energy in the deformation controlled zone. However, the mathematically flawless min-max form causes trouble for a gradient-based optimizer in a numerical process, because the min-max form is not differentiable. To overcome this problem, the maximum element strain energy Γ_{max} is approximated by an aggregation function in this study. Usually, the p-norm and Kreisselmeier-Steinhauser (KS) functions [38, 39] are available for aggregation. Without loss of generality, the p-norm function is used as

$$\begin{gathered} \Gamma_{\mathrm{max}} = \max(\Gamma_e | e \in \Theta) \approx g = \left(\sum_{e \in \Theta} \Gamma_e^p\right)^{(1/p)} \\ \Gamma_e = \boldsymbol{U}^{\mathrm{T}}\boldsymbol{K}_e\boldsymbol{U} = (\boldsymbol{U}_{\mathrm{N}} + \boldsymbol{U}_{\mathrm{V}})^{\mathrm{T}}\boldsymbol{K}_e(\boldsymbol{U}_{\mathrm{N}} + \boldsymbol{U}_{\mathrm{V}}) = \boldsymbol{U}_{\mathrm{N}}^{\mathrm{T}}\boldsymbol{K}_e\boldsymbol{U}_{\mathrm{N}} + \boldsymbol{U}_{\mathrm{V}}^{\mathrm{T}}\boldsymbol{K}_e\boldsymbol{U}_{\mathrm{V}} + 2\boldsymbol{U}_{\mathrm{N}}^{\mathrm{T}}\boldsymbol{K}_e\boldsymbol{U}_{\mathrm{V}} \end{gathered} \tag{5}$$

where Γ_e is the element strain energy of element e; p is the aggregation parameter that controls the performance of Eq. (5). When $p \to +\infty$, g approaches Γ_{max}. A good choice for p should therefore balance adequate smoothness and an appropriate approximation of Γ_{max}. A very large value of p requires more iteration steps to converge and brings in more oscillations in the objective value. Experimentally, $p = 8$ can yield good results in this study. In summary, the optimization problem can be formulated as

$$\begin{aligned} & \min_{\boldsymbol{\rho}}(g) \\ \text{s.t.} \quad & \boldsymbol{K}\boldsymbol{U}_{\mathrm{N}} = \boldsymbol{F}_{\mathrm{N}} \\ & \boldsymbol{K}\boldsymbol{U}_{\mathrm{V}} = \boldsymbol{F}_{\mathrm{V}} \\ & \frac{1}{V_{\mathrm{fra}}}\left(\frac{\sum_j V_j}{\sum_j V_{0,j}}\right) - 1 \leq 0, \qquad 0 \leq \rho_j \leq 1,\ j \in \Omega_{\mathrm{A}} \end{aligned} \tag{6}$$

where $V_{\mathrm{fra}} \in (0,1)$ is the volume fraction. Structural displacements $\boldsymbol{U}$ is calculated in an external finite element step using a nested approach.

3.4 Sensitivity analysis

Taking the derivative of g with respect to a design variable ρ_e yields the terms including the derivative of $\boldsymbol{U}_{\mathrm{N}}$ and $\boldsymbol{U}_{\mathrm{V}}$ with respect to ρ_e. The adjoint method, see [40] for a review, is employed to avoid directly solving

$\mathrm{d}\boldsymbol{U}_{\mathrm{N}}/\mathrm{d}\rho_e$ and $\mathrm{d}\boldsymbol{U}_{\mathrm{V}}/\mathrm{d}\rho_e$ in order to save computational cost. Thus, g is augmented into $\bar{g}$ with the multiplier vectors $\boldsymbol{\lambda}_1^{\mathrm{T}}$ and $\boldsymbol{\lambda}_2^{\mathrm{T}}$ as

$$\bar{g} = \left(\sum_{e\in\Theta} \Gamma_e^p\right)^{(1/p)} + \boldsymbol{\lambda}_1^{\mathrm{T}}(\boldsymbol{F}_{\mathrm{N}} - \boldsymbol{K}\boldsymbol{U}_{\mathrm{N}}) + \boldsymbol{\lambda}_2^{\mathrm{T}}(\boldsymbol{F}_{\mathrm{V}} - \boldsymbol{K}\boldsymbol{U}_{\mathrm{V}}) \tag{7}$$

According to the chain rule, the derivative of g with respect to ρ_e is given by

$$\frac{\mathrm{d}g}{\mathrm{d}\rho_e} = \sum_{i\in n_e}\left(\frac{\mathrm{d}g}{\mathrm{d}\bar{\rho}_i}\frac{\mathrm{d}\bar{\rho}_i}{\mathrm{d}\tilde{\rho}_i}\frac{\mathrm{d}\tilde{\rho}_i}{\mathrm{d}\rho_e}\right) \tag{8}$$

where $\mathrm{d}g/\mathrm{d}\bar{\rho}_e$ is expressed as below, according to the derivation in Appendix.

$$\frac{\mathrm{d}g}{\mathrm{d}\bar{\rho}_e} = -\boldsymbol{\lambda}_1^{\mathrm{T}}\frac{\mathrm{d}\boldsymbol{K}}{\mathrm{d}\rho_e}\boldsymbol{U}_{\mathrm{N}} - \boldsymbol{\lambda}_2^{\mathrm{T}}\frac{\mathrm{d}\boldsymbol{K}}{\mathrm{d}\rho_e}\boldsymbol{U}_{\mathrm{V}} \tag{9}$$

where $\boldsymbol{\lambda}_1$ and $\boldsymbol{\lambda}_2$ can be calculated through solving the following adjoint equations

$$\boldsymbol{K}^{\mathrm{T}}\boldsymbol{\lambda}_1 = 2\left[\sum_{e\in\Theta}\left(\frac{\mathrm{d}g}{\mathrm{d}\Gamma_e}\boldsymbol{K}_e\right)\right]\boldsymbol{U}, \qquad \boldsymbol{K}^{\mathrm{T}}\boldsymbol{\lambda}_2 = 2\left[\sum_{e\in\Theta}\left(\frac{\mathrm{d}g}{\mathrm{d}\Gamma_e}\boldsymbol{K}_e\right)\right]\boldsymbol{U} \tag{10}$$

Note that boundary conditions should be consistent with those in Fig. 2(b) and (c) when solving $\boldsymbol{\lambda}_1$ and $\boldsymbol{\lambda}_2$ in Eq. (10), respectively. Therefore, $\boldsymbol{\lambda}_1 \neq \boldsymbol{\lambda}_2$.

4. Optimization results

4.1 Deformation controlled zone and volume fraction

The ratio of axial compression stress to strength δ_{N}, which is also called 'axial compression ratio', and the demension in height H_{W} are fixed as 0.2 and 3.6m, respectively, to invetigate the effect of deformation controlled zone Θ and volume fraction V_{fra} in optimization process. The element strain energy contour of a reference half-structure in a conventional configuration is shown in Fig. 3. Obviously, the severest deformation locates the wall toe. The Young's modulus and thickness in the passive domain are different from those in the active domain. As a result, directly visualizing element strain energy from the two domians cannot present a clear intuion of deformation intensity. To fairly display deformation intensity and distribtion, element strain energy is nomralized by element thickness and Young's modulus as $\tilde{\Gamma}_e = \Gamma_e/(t_{\mathrm{c}}E_{\mathrm{c}})$ for $e \in \Omega_{\mathrm{P}}$ and $\tilde{\Gamma}_e = \Gamma_e/(t_{\mathrm{s}}E_{\mathrm{s}})$ for $e \in \Omega_{\mathrm{A}}$. Also, gain ratio ξ_g is defined as $\xi_g = (\Gamma_{\mathrm{max,ref}} - \Gamma_{\mathrm{max}})/\Gamma_{\mathrm{max,ref}}$ to quantify the benifit of optimization.

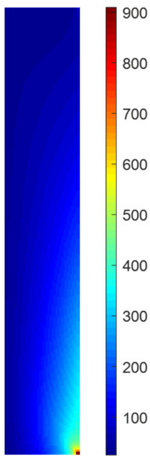

Fig. 3 – Element strain energy contour of a reference half-structure (unit for the color bar is [N·mm])

The variation of deformation controlled zone is manipulated via a index $\gamma_{\Theta} = H_{\Theta}/H_{\mathrm{W}}$. Deformation controlled zone shown in Fig. 2(d) has a noticeable effect on optimized results, as well as volume fraction V_{fra} referred in Eq. (6) according to the optimized results in Table 1. Optimized results converge to different configrations under $\gamma_{\Theta} = 0.25$, 0.50 and 0.75. When $\gamma_{\Theta} = 0.25$, severe deformation concentrates at the top conatct points between replaceable components and structural walls. Gain ratio is nonlinearly proportional to the allowable area of replaceable components according to the tendency depicted in Fig. 4. In the case of $\gamma_{\Theta} = 0.25$, gain ratio decreases, though consuming more material. Observations from numerical tests indicate that optimizations under $\gamma_{\Theta} = 0.75$ yield better results. The objective value in Fig. 5 descends as iteration number increases. The gain ratio histroy, the red line in Fig. 5, experiences a shape rise and then ascends slowly before weak oscillations. The trends of the objective value and gain raio conincide with each other. It demostrates that the p-norm function adequately approximates the maximum element strain energy $\Gamma_{\max}$ in a deformation controlled zone and the suggested optimization scheme performs well.

Table 1 – Optimized results from varying deformation controlled zone and volume fraction

Optimized configuration & $\tilde{\Gamma}_e$	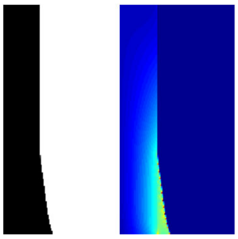	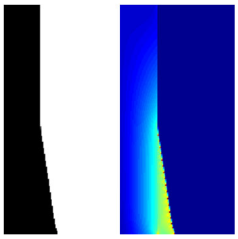	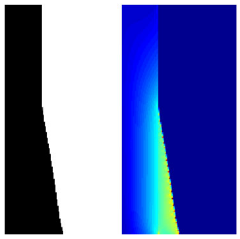
$\gamma_{\Theta}, \delta_{\mathrm{N}}$	0.75, 0.20		
V_{fra}	0.025	0.050	0.075
$\Gamma_{\max}$	335	267	223
ξ_g	0.63	0.71	0.75
Optimized configuration & $\tilde{\Gamma}_e$	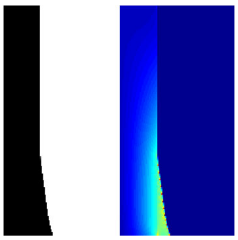	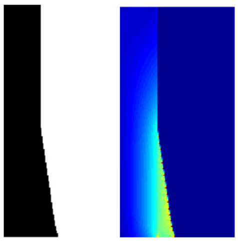	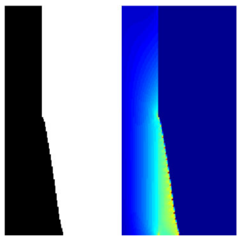
$\gamma_{\Theta}, \delta_{\mathrm{N}}$	0.50, 0.20		
V_{fra}	0.025	0.050	0.075
$\Gamma_{\max}$	335	267	266
ξ_g	0.63	0.71	0.71
Optimized configuration & $\tilde{\Gamma}_e$	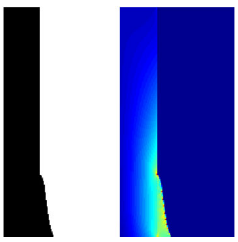	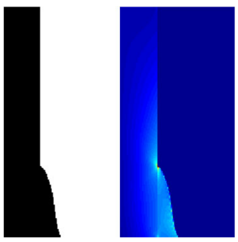	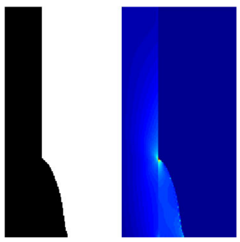
$\gamma_{\Theta}, \delta_{\mathrm{N}}$	0.25, 0.20		
V_{fra}	0.025	0.050	0.075
$\Gamma_{\max}$	490	585	605
ξ_g	0.46	0.36	0.33

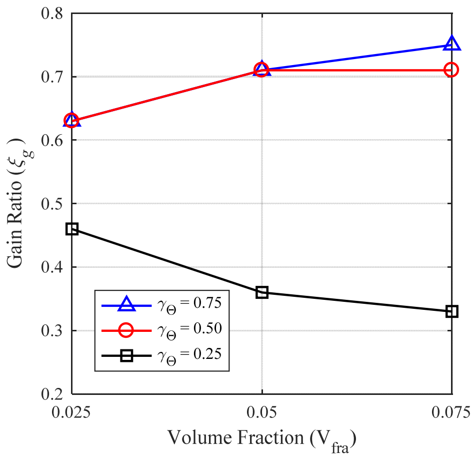

Fig. 4 – Tendency of gain ratio with respect to volume fraction

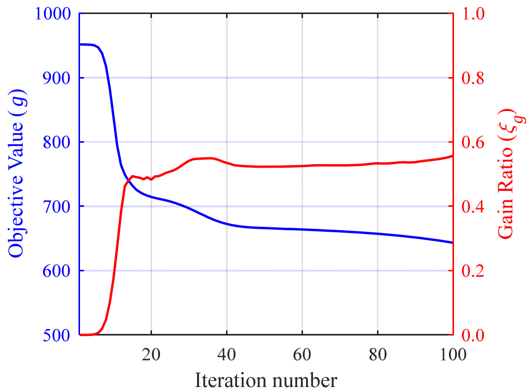

Fig. 5 – Histories of objective value and gain ratio in a optimization process

4.2 Axial compression ratio and aspect ratio

The effect of axial compression ratio $\boldsymbol{\delta}_{\mathrm{N}}$ on optimization results is investigated by varying from 0.0 to 0.5 at an interval of 0.1 on the one hand, and the optimization results also show a great dispartiy under different aspect ratios on the other hand, see details in Table 2. To yield reasonable results, deformation controlled zone is invarient as $\gamma_\Theta = 0.75$. The allowable in-plane area for replaceable components is set as 0.108m^2. Different aspect ratios are achieved in numerical tests by changing the geometry dimension in height at 1.2m, 2.4m and 3,6m.

In all cases, the gain ratios are larger than 0.4. It means that deformation intensity in the passive domain is significantly reduced by adding optimized replaceable components. Also, the deformation intensity in the optimized replaceable components is higher than that in the passive domain representing a reinfored concres structral wall. However, this effect is gradually reduced as axial compression ratio increases. The optimization efficacy is diluted by axial loads. Axial compression ratio also shapes the optimized configurations.

The effect of aspect ratio also affects geometries of replaceable components. In the case of aspect ratio equal to 3 (H_W = 3.6m and B_W = 1.2m), optimized components are similar to narrow and long wedges. The optimization efficacy is more pronounced in a situation where aspect ratio is close to 1. Fortunately, this decay shows a stable tendency. Overall, optimizatio allocates more material at the bottom section. The obtained configurations of replaceable components follow the conception of haunches in beam-to-column joints but the optimized geometries successfully balacne the stiffness contribution from the passive domain and the active domian to minimize the maximum element strain energy in deformation controlled zone.

Table 2 – Optimized results from varying axial compression ratio and aspect ratio

H_W = 1.2 (m)	**Optimized configuration**						
	$\tilde{\Gamma}_e$	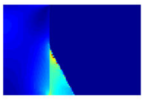	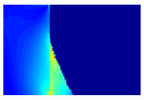	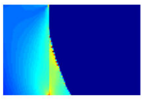	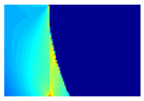	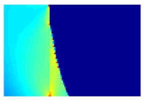	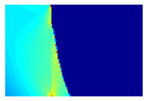
	δ_N	0.0	0.1	0.2	0.3	0.4	0.5
	$\Gamma_{max,ref}$	71	160	283	441	634	861
	Γ_{max}	17	48	96	180	311	479
	ξ_g	0.76	0.70	0.66	0.59	0.51	0.44
H_W = 2.4 (m)	**Optimized configuration**						
	$\tilde{\Gamma}_e$	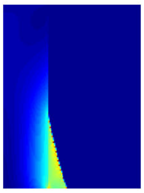	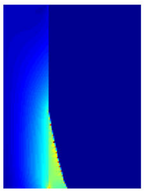	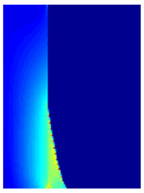	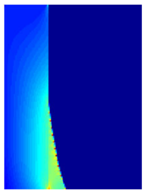	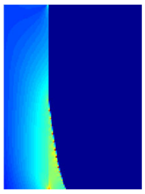	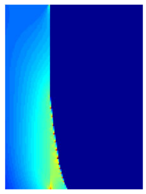
	δ_N	0.0	0.1	0.2	0.3	0.4	0.5
	$\Gamma_{max,ref}$	229	373	552	766	1015	1299
	Γ_{max}	66	121	192	284	391	514
	ξ_g	0.71	0.68	0.65	0.63	0.62	0.60
H_W = 3.6 (m)	**Optimized configuration**						
	$\tilde{\Gamma}_e$	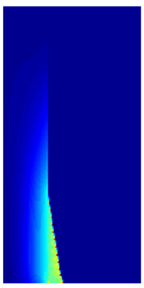	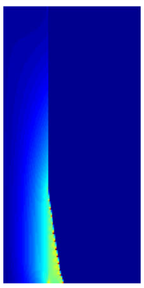	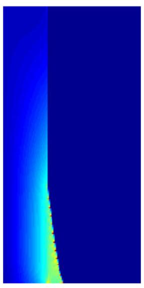	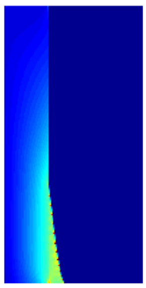	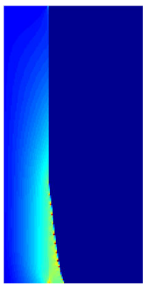	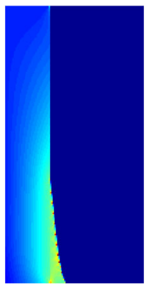
	δ_N	0.0	0.1	0.2	0.3	0.4	0.5
	$\Gamma_{max,ref}$	475	674	909	1179	1483	1823
	Γ_{max}	156	237	335	453	586	737
	ξ_g	0.67	0.65	0.63	0.62	0.60	0.60

5. Conclusions

A topology optimization scheme is proposed in this study to design replaceable components in structural walls. The maximum element strain energy in a numerical structural wall model can be considerablely decreased by 40 to 60 percent compared with conventional structural walls in the range of aspect ratio from 1 to 3. The replaceable component deforms more severely than the structural wall in the presented optimization results. The optimized configurations of replaceable components have concise shapes and like haunches in beam-to-column joints. Consequently, it never causes complexity in manufacuring.

Deformation controlled zone should be reasonablely set in optimization, otherwise optimization results would still suffer from concentrated deformation. Both axial compression ratio and aspect ratio affect the optimized configurations of replaceable components. According to the parameter study, gain ratio decays when axial compression ratio ascends. Gain ratio also decreases as aspect raio increases.

Acknowledgements

The authors acknowledge support from the National Natural Science Foundation of China under Grant No. 51638012. The MMA code from Professor Krister Svanberg (Department of Mathematics, KTH Royal Institute of Technology) is gratefully acknowledged.

Appendix

The derivative of element strain energy Γ_e with respect to a design variable ρ_e is calculated as below

$$\frac{\mathrm{d}\Gamma_e}{\mathrm{d}\rho_e}=\frac{\partial\Gamma_e}{\partial\boldsymbol{U}_\mathrm{N}}\frac{\mathrm{d}\boldsymbol{U}_\mathrm{N}}{\mathrm{d}\rho_e}+\frac{\partial\Gamma_e}{\partial\boldsymbol{U}_\mathrm{V}}\frac{\mathrm{d}\boldsymbol{U}_\mathrm{V}}{\mathrm{d}\rho_e}+\frac{\partial\Gamma_e}{\partial\rho_e}=2\boldsymbol{U}^\mathrm{T}\boldsymbol{K}_e\frac{\mathrm{d}\boldsymbol{U}_\mathrm{N}}{\mathrm{d}\rho_e}+2\boldsymbol{U}^\mathrm{T}\boldsymbol{K}_e\frac{\mathrm{d}\boldsymbol{U}_\mathrm{V}}{\mathrm{d}\rho_e}+\boldsymbol{U}^\mathrm{T}\frac{\mathrm{d}\boldsymbol{K}_e}{\mathrm{d}\rho_e}\boldsymbol{U} \tag{11}$$

Taking derivative of $\bar{g}$ in Eq. (7) with respect to a design variable ρ_e yields

$$\begin{aligned}\frac{\mathrm{d}\bar{g}}{\mathrm{d}\rho_e}&=\sum_{e\in\Theta}\left(\frac{\mathrm{d}g}{\mathrm{d}\Gamma_e}\frac{\mathrm{d}\Gamma_e}{\mathrm{d}\rho_e}\right)+\boldsymbol{\lambda}_1^\mathrm{T}\left(\frac{\mathrm{d}\boldsymbol{F}_\mathrm{N}}{\mathrm{d}\rho_e}-\frac{\mathrm{d}\boldsymbol{K}}{\mathrm{d}\rho_e}\boldsymbol{U}_\mathrm{N}-\boldsymbol{K}\frac{\mathrm{d}\boldsymbol{U}_\mathrm{N}}{\mathrm{d}\rho_e}\right)+\boldsymbol{\lambda}_2^\mathrm{T}\left(\frac{\mathrm{d}\boldsymbol{F}_\mathrm{V}}{\mathrm{d}\rho_e}-\frac{\mathrm{d}\boldsymbol{K}}{\mathrm{d}\rho_e}\boldsymbol{U}_\mathrm{V}-\boldsymbol{K}\frac{\mathrm{d}\boldsymbol{U}_\mathrm{V}}{\mathrm{d}\rho_e}\right)\\&=\sum_{e\in\Theta}\left[\frac{\mathrm{d}g}{\mathrm{d}\Gamma_e}\left(\boldsymbol{U}^\mathrm{T}\frac{\mathrm{d}\boldsymbol{K}_e}{\mathrm{d}\rho_e}\boldsymbol{U}\right)\right]+\sum_{e\in\Theta}\left[\frac{\mathrm{d}g}{\mathrm{d}\Gamma_e}\left(2\boldsymbol{U}^\mathrm{T}\boldsymbol{K}_e\frac{\mathrm{d}\boldsymbol{U}_\mathrm{N}}{\mathrm{d}\rho_e}\right)\right]+\sum_{e\in\Theta}\left[\frac{\mathrm{d}g}{\mathrm{d}\Gamma_e}\left(2\boldsymbol{U}^\mathrm{T}\boldsymbol{K}_e\frac{\mathrm{d}\boldsymbol{U}_\mathrm{V}}{\mathrm{d}\rho_e}\right)\right]\\&\quad-\boldsymbol{\lambda}_1^\mathrm{T}\frac{\mathrm{d}\boldsymbol{K}}{\mathrm{d}\rho_e}\boldsymbol{U}_\mathrm{N}-\boldsymbol{\lambda}_1^\mathrm{T}\boldsymbol{K}\frac{\mathrm{d}\boldsymbol{U}_\mathrm{N}}{\mathrm{d}\rho_e}-\boldsymbol{\lambda}_2^\mathrm{T}\frac{\mathrm{d}\boldsymbol{K}}{\mathrm{d}\rho_e}\boldsymbol{U}_\mathrm{V}-\boldsymbol{\lambda}_2^\mathrm{T}\boldsymbol{K}\frac{\mathrm{d}\boldsymbol{U}_\mathrm{V}}{\mathrm{d}\rho_e}\\&=\sum_{e\in\Theta}\left[\frac{\mathrm{d}g}{\mathrm{d}\Gamma_e}\left(\boldsymbol{U}^\mathrm{T}\frac{\mathrm{d}\boldsymbol{K}_e}{\mathrm{d}\rho_e}\boldsymbol{U}\right)\right]-\boldsymbol{\lambda}_1^\mathrm{T}\frac{\mathrm{d}\boldsymbol{K}}{\mathrm{d}\rho_e}\boldsymbol{U}_\mathrm{N}-\boldsymbol{\lambda}_2^\mathrm{T}\frac{\mathrm{d}\boldsymbol{K}}{\mathrm{d}\rho_e}\boldsymbol{U}_\mathrm{V}\\&\quad+\left[\sum_{e\in\Theta}\left(2\frac{\mathrm{d}g}{\mathrm{d}\Gamma_e}\boldsymbol{U}^\mathrm{T}\boldsymbol{K}_e\right)-\boldsymbol{\lambda}_1^\mathrm{T}\boldsymbol{K}\right]\frac{\mathrm{d}\boldsymbol{U}_\mathrm{N}}{\mathrm{d}\rho_e}+\left[\sum_{e\in\Theta}\left(2\frac{\mathrm{d}g}{\mathrm{d}\Gamma_e}\boldsymbol{U}^\mathrm{T}\boldsymbol{K}_e\right)-\boldsymbol{\lambda}_2^\mathrm{T}\boldsymbol{K}\right]\frac{\mathrm{d}\boldsymbol{U}_\mathrm{V}}{\mathrm{d}\rho_e}\end{aligned} \tag{12}$$

In order to eliminate the term containing the implicit derivative of displacements, namely $\mathrm{d}\boldsymbol{U}_\mathrm{V}/\mathrm{d}\rho_e$ and $\mathrm{d}\boldsymbol{U}_\mathrm{N}/\mathrm{d}\rho_e$, the adjoint equation, Eq.(10), should be solved. Also, note that $\mathrm{d}\boldsymbol{F}_\mathrm{N}/\mathrm{d}\rho_e=\boldsymbol{0}$ and $\mathrm{d}\boldsymbol{F}_\mathrm{V}/\mathrm{d}\rho_e=\boldsymbol{0}$, and $\mathrm{d}\boldsymbol{K}_e/\mathrm{d}\rho_e=\boldsymbol{0}$ for $e\in\Theta$. Thus, $\mathrm{d}g/\mathrm{d}\rho_e$ is obtained as Eq. (9).

References

[1] National Research Council (2011): National earthquake resilience: research, implementation, and outreach. The National Academies Press: Washigton DC, p. 19-34.

[2] Perez FJ, Pessiki S, Sause R (2013): Experimental lateral load response of unbonded post-tensioned precast concrete walls. *ACI Structural Journal*, **110**(6), 1045-1055.

[3] Marriott D, Pampanin S, Bull D, *et al*. (2008): Dynamic testing of precast, post-tensioned rocking wall systems with alternative dissipating solutions. *Bulletin of the New Zealand Society for Earthquake Engineering*, **41**(2), 90-103.

[4] Lu X, Cui Y, Liu J, *et al.* (2015): Shaking table test and numerical simulation of a 1/2-scale self-centering reinforced concrete frame. *Earthquake Engineering & Structural Dynamics*, **44**(12), 1899-1917.

[5] Eatherton MR, Ma X, Krawinkler H, Deierlein GG, Hajjar JF (2014): Quasi-static cyclic behavior of controlled rocking steel frames. *Journal of Structural Engineering*, **140**(11), 04014083.

[6] Marriott D, Pampanin S, Palermo A (2009): Quasi-static and pseudo-dynamic testing of unbonded post-tensioned rocking bridge piers with external replaceable dissipaters. *Earthquake Engineering & Structural Dynamics*, **38**(3), 331-354.

[7] Pampanin S, Kam WY, Haverland G, *et al.* (2011): Seismic performance of a post-tensioned precast concrete building (PRESSS Technology) during the 22nd Feb 2011 Christchurch earthquake: reality check meets community expectations. Proc., NZ Concrete Industry Conference, New Zealand Concrete Society (NZCS).

[8] Gao W, Lu X (2019): Modelling unbonded prestressing tendons in self-centering connections through improved sliding cable elements. *Engineering Structures*, **180**(1), 809-828.

[9] Kim HJ, Christopoulos C (2009): Numerical models and ductile ultimate deformation response of post-tensioned self-centering moment connections. *Earthquake Engineering & Structural Dynamics*, **38**, 1-21.

[10] Lu X, Jiang C, *et al.* (2019): Seismic design methodology for self-centering reinforced concrete frames. *Soil Dynamics and Earthquake Engineering*, **119**, 358-374.

[11] Shen Y, Christopoulos C, Mansour N, Tremblay R (2011): Seismic design and performance of steel moment-resisting frames with nonlinear replaceable links. *Journal of Structural Engineering*, **137**, 1107-1117.

[12] Fortney PJ, Shahrooz BM, Rassati GA (2007): Large-scale testing of a replaceable fuse steel coupling beam. *Journal of Structural Engineering*, **133**, 1801-1807.

[13] Lu X, Chen C, Chen Y, Shan J (2016): Application of replaceable coupling beams to RC structures. *The Structural Design of Tall and Special Buildings*, **25**, 947-966.

[14] Lu X, Chen C, Jiang H, Wang S (2018): Shaking table tests and numerical analyses of an RC coupled wall structure with replaceable coupling beams. *Earthquake Engineering & Structural Dynamic*, **47**, 1882-1904.

[15] Lehman DE, Turgeon JA, Birely AC, *et al.* (2013): Seismic behavior of a modern concrete coupled wall. *Journal of Structural Engineering*, **139**, 1371-1381.

[16] Kam WY, Pampanin S (2011): The seismic performance of RC buildings in the 22 February 2011 Christchurch earthquake. *Structural Concrete*, **12**, 223-233.

[17] Wallace JW (2012): Behavior, design, and modeling of structural walls and coupling beams-lessons from recent laboratory tests and earthquakes. *International Journal of Concrete Structures and Materials*, **6**, 3-18.

[18] Lu X, Chen Y (2005): Modeling of coupled shear walls and its experimental verification. *Journal of Structural Engineering*, **131**, 75-84.

[19] Greifenhagen C, Lestuzzi P (2005): Static cyclic tests on lightly reinforced concrete shear walls. *Engineering Structures*, **27**, 1703-1712.

[20] Jiang H, Wang B, Lu X (2013): Experimental study on damage behavior of reinforced concrete shear walls subjected to cyclic loads. *Journal of Earthquake Engineering*, **17**, 958-971.

[21] Dashti F, Dhakal RP, Pampanin S (2017): Numerical modeling of rectangular reinforced concrete structural walls. *Journal of Structural Engineering*, **143**(6), 04017031.

[22] Lu X, Mao Y, Chen Y (2013): New structural system for earthquake resilient design. *Journal of Earthquake and Tsunami*, **7**(3), 1350013.

[23] Liu Q, Jiang H (2017): Experimental study on a new type of earthquake resilient shear wall. *Earthquake Engineering & Structural Dynamics*, **46**, 2479-2497.

[24] Bendsøe MP, Kikuchi N (1988) Generating optimal topologies in structural design using a homogenization method. *Computer Methods in Applied Mechanics and Engineering*, **71**(2), 197-224.

[25] Deaton JD, Grandhi RV (2014): A survey of structural and multidisciplinary continuum topology optimization: post 2000. *Structural and Multidisciplinary Optimization*, **49**(1), 1-38.

[26] Beghini LL, Beghini A, Katz N, Baker WF, Paulino GH (2014): Connecting architecture and engineering through structural topology optimization. *Engineering Structures*, **59**, 716-726.

[27] Pampanin S, Christopoulos C, Chen TH (2006): Development and validation of a metallic haunch seismic retrofit solution for existing under-designed RC frame buildings. *Earthquake Engineering and Structural Dynamics*, **35**, 1739-1766.

[28] Lee CH, Jung JH, Oh MH, Koo ES (2003): Cyclic seismic testing of steel moment connections reinforced with welded straight haunch. *Engineering Structure*, **25**, 1743-1753.

[29] Uang CM, Yu QS, Noel S, Gross J (2000): Cyclic testing of steel moment connections rehabilitated with RBS or welded haunch. *Journal of Structural Engineering*, **126**, 57-68.

[30] Bathe KJ (1996): *Finite element procedures*. Prentice hall, New Jersey.

[31] Zhou M, Rozvany G (1991): The COC algorithm, Part II: topological, geometrical and generalized shape optimization. *Computer Methods in Applied Mechanics Engineering*, **89**(1-3), 309-336.

[32] Andreassen E, Clausen A, Schevenels M, Lazarov B, Sigmund O (2011): Efficient topology optimization in matlab using 88 lines of code. *Structural and Multidisciplinary Optimization*, **43**(1), 1-16.

[33] Sigmund O (2001): A 99 line topology optimization code written in Matlab. *Structural and Multidisciplinary Optimization*, **21**(2), 120-127.

[34] Bendsøe M, Sigmund O (2003): *Topology optimization – theory, methods and applications*. Springer Verlag, Berlin.

[35] Wang F, Lazarov BS, Sigmund O (2011): On projection methods, convergence and robust formulations in topology optimization. *Structural and Multidisciplinary Optimization*, **43**(6), 767-784.

[36] Zhu JH, Li Y, Zhang WH (2016): Shape preserving design with structural topology optimization. *Structural and Multidisciplinary Optimization*, **53**(4), 893-906.

[37] Castro MS, Silva OM, Lenzi A, Neves MM (2018): Shape preserving design of vibrating structures using topology optimization. *Structural and Multidisciplinary Optimization*, **58**(3), 1109-1119.

[38] Li X (1991): An aggregate function method for nonlinear programming. Science in China, **34**(12), 1467-1473.

[39] Le C, Norato J, Bruns T, Ha C, Tortorelli D (2010): Stress-based topology optimization for continua. *Structural and Multidisciplinary Optimization*, **41**, 605-620.

[40] Tortorelli DA, Michaleris P (1994): Design sensitivity analysis: overview and review. *Inverse problems in Engineering*, **1**(1), 71-105.

